Commun. Comput. Phys.
doi: 10.4208/cicp.151214.021015a

Vol. **19**, No. 4, pp. 1067-1093
April 2016

Pseudo-Arclength Continuation Algorithms for Binary Rydberg-Dressed Bose-Einstein Condensates

Sirilak Sriburadet[1], Y.-S. Wang[2], C.-S. Chien[2,*] and Y. Shih[1]

[1] *Department of Applied Mathematics, National Chung Hsing University, Taichung 402, Taiwan.*
[2] *Department of Computer Science and Information Engineering, Chien Hsin University of Science and Technology, Zhongli 320, Taiwan.*

Received 15 December 2014; Accepted (in revised version) 2 October 2015

Abstract. We study pseudo-arclength continuation methods for both Rydberg-dressed Bose-Einstein condensates (BEC), and binary Rydberg-dressed BEC which are governed by the Gross-Pitaevskii equations (GPEs). A divide-and-conquer technique is proposed for rescaling the range/ranges of nonlocal nonlinear term/terms, which gives enough information for choosing a proper stepsize. This guarantees that the solution curve we wish to trace can be precisely approximated. In addition, the ground state solution would successfully evolve from one peak to vortices when the affect of the rotating term is imposed. Moreover, parameter variables with different number of components are exploited in curve-tracing. The proposed methods have the advantage of tracing the ground state solution curve once to compute the contours for various values of the coefficients of the nonlocal nonlinear term/terms. Our numerical results are consistent with those published in the literatures.

AMS subject classifications: 65N35, 35P30, 35Q55

Key words: Ground state solution, solution branch, spectral collocation method, divide-and-conquer..

1 Introduction

In this paper, we are concerned with pseudo-arclength continuation algorithms for computing numerical solutions of nonlinear eigenvalue problems of the following form

$$\mathbf{F}(\mathbf{x},\Lambda)=0, \tag{1.1}$$

where $\mathbf{F}:\mathbf{B_1}\times\mathbf{R}^m\to\mathbf{B_2}$ is a smooth mapping with $\mathbf{x}\in\mathbf{B_1}$, $\Lambda=(\lambda_1,\cdots,\lambda_m)\in\mathbf{R}^m$, $\mathbf{x}$ is the state variable, Λ is the parameter variable, and $\mathbf{B_1}$ and $\mathbf{B_2}$ are two Banach spaces. A

*Corresponding author. *Email addresses:* yuijungja@yahoo.com (S. Sriburadet), wang04.wang25@msa.hinet.net (Y.-S. Wang), cschien@uch.edu.tw (C.-S. Chien), Yintzer_Shih@nchu.edu.tw (Y. Shih)

 ©2016 Global-Science Press

https://doi.org/10.4208/cicp.151214.021015a Published online by Cambridge University Press

typical example of Eq. (1.1) is the Gross-Pitaevskii equation (GPE), where the parameters $\lambda_i, 1\leq i\leq m$, have specific physical meaning.

Recently, it has been observed that a quantum system of interacting particles can exhibit both crystalline structure and superfluid property [1, 2]. Henkel *et al*. [3] showed that the particles of Bose-Einstein condensates (BEC) interacting through an isotropically repulsive van der Waals interaction with a softened core might support a density modulation. They observed that spontaneously crystalline ground states, called quantum crystals, could exist on trapped Rydberg-dressed BEC. Based on the mean-field theory, we consider two-component (rotating) Rydberg-dressed BEC which is governed by the coupled GPEs of the following form:

$$\begin{aligned}
\mathbf{i}\partial_t\Psi_1(\mathbf{r},t) &= \Big[-\frac{1}{2}\nabla^2+V(\mathbf{r})+\gamma_{11}|\Psi_1(\mathbf{r},t)|^2+\gamma_{12}|\Psi_2(\mathbf{r},t)|^2+\mu_{11}\int\frac{|\Psi_1(\mathbf{r}',t)|^2}{1+|\mathbf{r}-\mathbf{r}'|^6}d\mathbf{r}' \\
&\quad +\mu_{12}\int\frac{|\Psi_2(\mathbf{r}',t)|^2}{1+|\mathbf{r}-\mathbf{r}'|^6}d\mathbf{r}'-\omega L_z\Big]\Psi_1(\mathbf{r},t), \quad t>0, \\
\mathbf{i}\partial_t\Psi_2(\mathbf{r},t) &= \Big[-\frac{1}{2}\nabla^2+V(\mathbf{r})+\gamma_{22}|\Psi_2(\mathbf{r},t)|^2+\gamma_{21}|\Psi_1(\mathbf{r},t)|^2+\mu_{22}\int\frac{|\Psi_2(\mathbf{r}',t)|^2}{1+|\mathbf{r}-\mathbf{r}'|^6}d\mathbf{r}' \\
&\quad +\mu_{21}\int\frac{|\Psi_1(\mathbf{r}',t)|^2}{1+|\mathbf{r}-\mathbf{r}'|^6}d\mathbf{r}'-\omega L_z\Big]\Psi_2(\mathbf{r},t), \quad t>0,
\end{aligned} \tag{1.2}$$

where (Ψ_1,Ψ_2) is the vector of two-component complex wave functions, $V(\mathbf{r})=\eta^2\mathbf{r}^2/2$ is the harmonic trapping potential with η the radius frequency and $\mathbf{r}\in\mathbf{R}^n, n=2,3$, γ_{jj} $(j=1,2)$ and γ_{jl} $(j,l=1,2)$ are the short-range intra-component interactions and inter-component interactions in the two-component BECs, respectively, μ_{jj} $(j=1,2)$ and μ_{jl} $(j,l=1,2)$ are the long-range intra-component interactions and inter-component interactions in the two-component BECs, or the coefficients of the nonlocal nonlinear terms, respectively, ω is an angular velocity, and $L_z=xp_y-yp_x=-\mathbf{i}(x\partial y-y\partial x)$ is the z-component of the angular momentum $\mathbf{L}=\mathbf{r}\times\mathbf{P}$ with the momentum operator $\mathbf{P}=-\mathbf{i}\nabla=(p_x,p_y,p_z)^T$. A special case of Eq. (1.2) is the one-component Rydberg-dressed BEC which is governed by the GPE of the following form:

$$\mathbf{i}\partial_t\Psi(\mathbf{r},t)=\Big[-\frac{1}{2}\nabla^2+V(\mathbf{r})+\gamma|\Psi(\mathbf{r},t)|^2+\mu\int\frac{|\Psi(\mathbf{r}',t)|^2}{1+|\mathbf{r}-\mathbf{r}'|^6}d\mathbf{r}'-\omega L_z\Big]\Psi(\mathbf{r},t), \tag{1.3}$$

where the parameters used in Eq. (1.3) have the same physical meaning as those used in Eq. (1.2). Substituting the formula

$$\Psi_j(\mathbf{r},t)=e^{-\mathbf{i}\lambda_j t}\psi_j(\mathbf{r}), \quad j=1,2$$

into Eq. (1.2), we obtain the coupled stationary state nonlinear eigenvalue problem

$$\begin{aligned}
F_1(\psi_1,\psi_2,\lambda_1,\lambda_2) &= \Big[-\frac{1}{2}\nabla^2+V(\mathbf{r})+\gamma_{11}|\psi_1(\mathbf{r})|^2+\gamma_{12}|\psi_2(\mathbf{r})|^2+\mu_{11}\int\frac{|\psi_1(\mathbf{r}')|^2}{1+|\mathbf{r}-\mathbf{r}'|^6}d\mathbf{r}' \\
&\quad +\mu_{12}\int\frac{|\psi_2(\mathbf{r}')|^2}{1+|\mathbf{r}-\mathbf{r}'|^6}d\mathbf{r}'-\omega L_z-\lambda_1\Big]\psi_1(\mathbf{r})=0,
\end{aligned}$$

https://doi.org/10.4208/cicp.151214.021015a Published online by Cambridge University Press

$$F_2(\psi_1,\psi_2,\lambda_1,\lambda_2)=\Big[-\frac{1}{2}\nabla^2+V(\mathbf{r})+\gamma_{22}|\psi_2(\mathbf{r})|^2+\gamma_{21}|\psi_1(\mathbf{r})|^2+\mu_{22}\int\frac{|\psi_2(\mathbf{r}')|^2}{1+|\mathbf{r}-\mathbf{r}'|^6}d\mathbf{r}'$$
$$+\mu_{21}\int\frac{|\psi_1(\mathbf{r}')|^2}{1+|\mathbf{r}-\mathbf{r}'|^6}d\mathbf{r}'-\omega L_z-\lambda_2\Big]\psi_2(\mathbf{r})=0,$$
$$\psi_j(\mathbf{r})=0 \text{ on } \partial\Omega, \quad j=1,2, \tag{1.4}$$

with the normalization conditions

$$\int_\Omega|\psi_j(\mathbf{r})|^2d\mathbf{r}=1, \quad j=1,2. \tag{1.5}$$

Here λ_1 and λ_2 are the chemical potentials of the condensates, $\psi_1(\mathbf{r})$ and $\psi_2(\mathbf{r})$ are the complex wave functions independent of the time variable t. Similarly, substituting the formula

$$\Psi(\mathbf{r},t)=e^{-\mathbf{i}\lambda t}\psi(\mathbf{r})$$

into Eq. (1.3), we obtain the associated stationary state nonlinear eigenvalue problem

$$F(\psi,\lambda)=\Big[-\frac{1}{2}\nabla^2+V(\mathbf{r})+\gamma|\psi(\mathbf{r})|^2+\mu\int\frac{|\psi(\mathbf{r}')|^2}{1+|\mathbf{r}-\mathbf{r}'|^6}d\mathbf{r}'-\omega L_z-\lambda\Big]\psi(\mathbf{r})=0, \quad \mathbf{r}\in\Omega,$$
$$\psi(\mathbf{r})=0 \text{ on } \partial\Omega, \tag{1.6}$$

with the normalization condition

$$\int_\Omega|\psi(\mathbf{r})|^2d\mathbf{r}=1. \tag{1.7}$$

Here λ is the chemical potential of the condensates, $\psi(\mathbf{r})$ is the complex wave function independent of the time variable t.

Recently, Henkel *et al*. [4] studied rotating quasi-two-dimensional BEC, in which atoms are dressed to a highly excited Rydberg state. Hsueh *et al*. [5] used the Fourier pseudo-spectral method combined with the adaptive Runge-Kutta method of order two and three (RK23) to compute the ground state solutions of Eq. (1.3) with $\gamma=0$, where the integral term was evaluated by the Fast Fourier transform (FFT). Actually, various numerical methods have been proposed for solving various types the GPE [6–10]. Specifically, García-Ripoll and Pérez-García [11] applied the Sobolev gradients method to compute the ground state solution of rotating BEC, where the Sobolev gradients were used as the preconditioner for the classical steepest descent methods (SDM), or the so-called imaginary time evolution method, and the free energy. Bao and Du [12] studied a continuous normalized gradient flow (CNGF) for computing the ground state solution of BEC. The idea of CNGF was extended to compute numerical solutions of multi-component BEC [13] and rotating BEC [14]. Moreover, the Fourier sine functions have been used as the basis functions combined with Euler scheme for computing ground state solutions of BEC and spin-1 BEC by Bao *et al*. [15], and Bao and Lim [16], respectively. Recently,

https://doi.org/10.4208/cicp.151214.021015a Published online by Cambridge University Press

Danaila and Kazemi [17] proposed a new improvement for the SDM to solve rotating BEC in two levels.

The coupled GPEs (1.2) is a system of nonlinear elliptic eigenvalue problem with physical parameters of different ranges. These parameters are given to determine locations of ground state solutions or excited state solutions. Since the eighties of last century it is well-known that continuation methods are efficient numerical methods for solving nonlinear elliptic eigenvalue problems. See, e.g., [18–20]. Therefore one can use pseudo-arclength continuation methods to trace one-dimensional solution curves of the GPE [18, p. 36; 19, p. 4]. For certain nonlinear elliptic eigenvalue problems with multiple parameters, one may be interested in finding solution manifolds described by some parameters of the physical system. See, e.g., [21–24] and further references cited therein. During the past decade, some continuation methods have been applied to compute numerical solutions of BEC. See, e.g., [25–31].

In this paper, we study divide-and-conquer pseudo-arclength continuation algorithms combined with a spectral collocation method (SCM) for computing numerical solutions of Eqs. (1.4) and (1.6), where the Fourier sine functions are used as the basis functions for the trial function space. When the contour of the solution starts to evolve from one peak (with ring structure) to a hexagonal crystal structure where $\omega = 0$, or to vortices where $\omega \in (0,1)$, it might happen that Newton's method would diverge or converge to a nearby solution branch without physical meaning if the steplength is improperly chosen. On the other hand, if the steplength is too small, then the evolution of one peak to a hexagonal crystal structure or to vortices would become impossible. Under such circumstance we need a divide-and-conquer technique to rescale the range of the nonlocal nonlinear term so that the solution branch can be well approximated. More precisely, for one-component BEC we rescale the interval $[0,\mu^*]$ for the coefficient of the integral term to the unit interval $[0,1]$, where the parameter μ is replaced by $\nu \in [0,1]$. Then we choose $\Lambda = (\lambda,\nu)$ as the parameter variable for continuation. For two-component BEC, we use the same technique to rescale the ranges of inter-component interactions and intra-component interactions and define two artificial parameters ν_0 and ν_1, respectively. Then we propose a pseudo-arclength continuation algorithm with the parameter variable $\Lambda = (\lambda_1,\lambda_2,\nu_0,\nu_1) \in \mathbf{R}^4$ for curve-tracing, where the splitting of the tangent vector for both components, and the normalization conditions (1.5) are used as the four constraint conditions. We observe that the parameters μ_{jj} reach the maximum value earlier than μ_{jl}. Thus we can reduce the dimension of the parameter variable Λ to $\Lambda_1 = (\lambda_1,\lambda_2,\nu_0) \in \mathbf{R}^3$, and proceed to trace the solution curve until the desired ground state solutions are obtained.

This paper is organized as follows. In Section 2 we study the SCM for binary rotating Rydberg-dressed BEC. In Section 3 we briefly discuss the continuation method described in [32] for binary rotating Rydberg-dressed BEC, where the parameter variable consists of two components λ_1 and λ_2 only. In Section 4 we propose divide-and-conquer pseudo-arclength continuation algorithms for rescaling the ranges/range of nonlocal nonlinear terms/term of Eqs. (1.4) and (1.6). Comprehensive numerical experiments for these two equations are reported in Section 5 where both 2D and 3D problems were studied. The

https://doi.org/10.4208/cicp.151214.021015a Published online by Cambridge University Press

numerical results are consistent with those published in the literatures [5,33]. Finally, an analysis of the numerical results and some concluding remarks are given in Section 6.

2 A SCM for binary rotating Rydberg-dressed BEC

For convenience we consider Eq. (1.4) in two-dimension. The 3D problem is a straight forward extension of the 2D case. We rewrite Eq. (1.4) as

$$\begin{aligned}
F_1(\psi_1,\psi_2,\lambda_1,\lambda_2) &= \Big[-\frac{1}{2}\Delta+V(\mathbf{r})+\gamma_{11}U(\psi_1)+\gamma_{12}U(\psi_2)+\mu_{11}\Phi(\psi_1)+\mu_{12}\Phi(\psi_2)\\
&\quad -\omega L_z-\lambda_1\Big]\psi_1=0,\\
F_2(\psi_1,\psi_2,\lambda_1,\lambda_2) &= \Big[-\frac{1}{2}\Delta+V(\mathbf{r})+\gamma_{22}U(\psi_2)+\gamma_{21}U(\psi_1)+\mu_{22}\Phi(\psi_2)+\mu_{21}\Phi(\psi_1)\\
&\quad -\omega L_z-\lambda_2\Big]\psi_2=0,\\
&\quad \mathbf{r}\in\Omega=(-l,l)^2,\quad \psi_j(\mathbf{r})=0 \text{ on } \partial\Omega,\quad j=1,2.
\end{aligned} \tag{2.1}$$

Here

$$U(\psi_j)=|\psi_j(\mathbf{r})|^2,\quad j=1,2, \tag{2.2}$$

and

$$\Phi(\psi_j)=\int g(\mathbf{r}-\mathbf{r}')|\psi_j(\mathbf{r}')|^2d\mathbf{r}'=\mathcal{F}^{-1}\big[\mathcal{F}[g(\mathbf{r})]\cdot\mathcal{F}[|\psi_j(\mathbf{r})|^2]\big],\quad j=1,2, \tag{2.3}$$

with

$$g(\mathbf{r})=\frac{1}{1+|\mathbf{r}|^6}$$

are the nonlinear terms with $\mathcal{F}$ and $\mathcal{F}^{-1}$ denoting the Fourier transform and inverse Fourier transform, respectively. Let $\psi_j(\mathbf{r})=u_j(\mathbf{r})+\mathbf{i}v_j(\mathbf{r}),j=1,2$ in Eq. (2.1), where $u_j(\mathbf{r})$ and $v_j(\mathbf{r})$ are two real-valued functions. Eq. (2.1) can be written as

$$\begin{aligned}
\widetilde{F}_1(u_1,v_1,u_2,v_2,\lambda_1,\lambda_2) &= \Big[-\frac{1}{2}\Delta+V(\mathbf{r})+\gamma_{11}\tilde{U}(u_1,v_1)+\gamma_{12}\tilde{U}(u_2,v_2)+\mu_{11}\tilde{\Phi}(u_1,v_1)\\
&\quad +\mu_{12}\tilde{\Phi}(u_2,v_2)-\lambda_1\Big]u_1-\omega(x(v_1)_y-y(v_1)_x)=0,\\
\widetilde{F}_2(u_1,v_1,u_2,v_2,\lambda_1,\lambda_2) &= \Big[-\frac{1}{2}\Delta+V(\mathbf{r})+\gamma_{11}\tilde{U}(u_1,v_1)+\gamma_{12}\tilde{U}(u_2,v_2)+\mu_{11}\tilde{\Phi}(u_1,v_1)\\
&\quad +\mu_{12}\tilde{\Phi}(u_2,v_2)-\lambda_1\Big]v_1+\omega(x(u_1)_y-y(u_1)_x)=0,\\
\widetilde{F}_3(u_1,v_1,u_2,v_2,\lambda_1,\lambda_2) &= \Big[-\frac{1}{2}\Delta+V(\mathbf{r})+\gamma_{22}\tilde{U}(u_2,v_2)+\gamma_{21}\tilde{U}(u_1,v_1)+\mu_{22}\tilde{\Phi}(u_2,v_2)\\
&\quad +\mu_{21}\tilde{\Phi}(u_1,v_1)-\lambda_2\Big]u_2-\omega(x(v_2)_y-y(v_2)_x)=0,
\end{aligned}$$

https://doi.org/10.4208/cicp.151214.021015a Published online by Cambridge University Press

$$\widetilde{F}_4(u_1,v_1,u_2,v_2,\lambda_1,\lambda_2)=\Big[-\frac{1}{2}\Delta+V(\mathbf{r})+\gamma_{22}\tilde{U}(u_2,v_2)+\gamma_{21}\tilde{U}(u_1,v_1)+\mu_{22}\tilde{\Phi}(u_2,v_2)$$
$$+\mu_{21}\tilde{\Phi}(u_1,v_1)-\lambda_2\Big]v_2+\omega(x(u_2)_y-y(u_2)_x)=0, \tag{2.4}$$

where

$$\tilde{U}(u_j,v_j)=u_j^2+v_j^2, \tag{2.5}$$

and

$$\tilde{\Phi}(u_j,v_j)=\int g(\mathbf{r}-\mathbf{r}')(u_j^2(\mathbf{r}')+v_j^2(\mathbf{r}'))d\mathbf{r}'$$
$$=\mathcal{F}^{-1}\big[\mathcal{F}[g(\mathbf{r})]\cdot\mathcal{F}[u_j^2(\mathbf{r})+v_j^2(\mathbf{r})]\big],\quad j=1,2. \tag{2.6}$$

Recently, the Fourier sine functions were used as the basis functions for computing numerical solutions of rotating BEC [15, 30], and the ground state solutions of dipolar BEC [34]. In this paper, we will use the Fourier sine functions as the basis functions for the SCM to compute the ground state solutions of binary rotating Rydberg-dressed BEC. First, we transform the domain $\Omega=(-l,l)^2$ in Eq. (2.4) into $\widetilde{\Omega}=(0,1)^2$ using the change of variables. Let

$$V_N^2=span\{\sin i\pi x\sin j\pi y\,|\,i,j=1,2,\cdots,N,x,y\in[0,1]\}$$

be the trial function space. All functions of V_N^2 satisfy the boundary condition $\psi|_{\partial\widetilde{\Omega}}=0$. To simplify the notations, we will use Eq. (2.4) to denote the new equation. The SCM for Eq. (2.4) is to find the following approximate solutions

$$u_1^N(x,y)=\sum_{i,j=1}^{N}\alpha_{ij}\sin i\pi x\sin j\pi y,\ v_1^N(x,y)=\sum_{i,j=1}^{N}\beta_{ij}\sin i\pi x\sin j\pi y\in V_N^2,$$
$$u_2^N(x,y)=\sum_{i,j=1}^{N}\tilde{\alpha}_{ij}\sin i\pi x\sin j\pi y,\ v_2^N(x,y)=\sum_{i,j=1}^{N}\tilde{\beta}_{ij}\sin i\pi x\sin j\pi y\in V_N^2, \tag{2.7}$$

where the integral terms in Eq. (2.6) are computed by the FFT. The nonlinear system associated with Eq. (2.4) can be expressed as

$$H(\alpha,\beta,\tilde{\alpha},\tilde{\beta},\lambda_1,\lambda_2):=H(\mathbf{x},\Lambda)=\big[H_1(\mathbf{x},\Lambda),H_2(\mathbf{x},\Lambda),H_3(\mathbf{x},\Lambda),H_4(\mathbf{x},\Lambda)\big]^T=0, \tag{2.8}$$

where $H:\mathbf{R}^{4N^2+2}\to\mathbf{R}^{4N^2}$ is a smooth mapping with the four components $H_j,j=1,2,3,4$, $\Lambda=(\lambda_1,\lambda_2)$ is the parameter variable, and $\mathbf{x}=(\alpha,\beta,\tilde{\alpha},\tilde{\beta})$ is the state variable, where

$$\alpha=[\alpha_{1,1},\cdots,\alpha_{1,N},\cdots,\alpha_{N,1},\cdots,\alpha_{N,N}]^T,\quad \beta=[\beta_{1,1},\cdots,\beta_{1,N},\cdots,\beta_{N,1},\cdots,\beta_{N,N}]^T\in\mathbf{R}^{N^2},$$
$$\tilde{\alpha}=[\tilde{\alpha}_{1,1},\cdots,\tilde{\alpha}_{1,N},\cdots,\tilde{\alpha}_{N,1},\cdots,\tilde{\alpha}_{N,N}]^T,\quad \tilde{\beta}=[\tilde{\beta}_{1,1},\cdots,\tilde{\beta}_{1,N},\cdots,\tilde{\beta}_{N,1},\cdots,\tilde{\beta}_{N,N}]^T\in\mathbf{R}^{N^2},$$

are the unknown coefficients yet to be determined. The Jacobian matrix associated with H is denoted by $DH\in\mathbf{R}^{4N^2\times(4N^2+2)}$.

https://doi.org/10.4208/cicp.151214.021015a Published online by Cambridge University Press

3 A brief review of the continuation algorithm

The continuation algorithm described in [32] is designed mainly for computing numerical solutions of rotating two-component BEC in optical lattices. In this section we will adapt the idea of that algorithm for computing the ground state solution of Eq. (1.4). A solution curve of Eq. (2.8) is denoted by

$$c=\{\mathbf{y}(s)=(\alpha(s),\beta(s),\tilde{\alpha}(s),\tilde{\beta}(s),\lambda_1(s),\lambda_2(s))\,|\,H(\mathbf{y}(s))=0,s\in I\subset\mathbf{R}\}.$$

Assume that a parametrization via arclength is available on the solution curve c.

The main idea of numerical continuation methods for computing the ground state solution of BEC is to use the energy level of the Schrödinger eigenvalue problem (SEP) to approximate the energy level of the GPE [25]. To compute the ground state solution, we use the pseudo-arclength predictor-corrector continuation method to trace the solution curve of Eq. (2.4) branching from the first bifurcation point $(0,0,0,0,\tilde{\lambda}_1,\tilde{\lambda}_2)$ of the GPEs, which is the minimum eigenvalue of the SEP [25,26,30–32,34]. Differentiating $H(\mathbf{y}(s))=0$ with respect to s, we obtain

$$DH(\mathbf{y}(s))\cdot\dot{\mathbf{y}}(s)=0, \tag{3.1}$$

where $\dot{\mathbf{y}}=(\dot{\alpha}(s),\dot{\beta}(s),\dot{\tilde{\alpha}}(s),\dot{\tilde{\beta}}(s),\dot{\lambda_1}(s),\dot{\lambda_2}(s))^T$ is the unit tangent vector to the solution curve c at $\mathbf{y}(s)$ and

$$DH(\mathbf{y}(s))=\left(D_\alpha H,D_\beta H,D_{\tilde{\alpha}}H,D_{\tilde{\beta}}H,D_{\lambda_1}H,D_{\lambda_2}H\right)\in\mathbf{R}^{4N^2\times(4N^2+2)} \tag{3.2}$$

has full rank. Here we have omitted the variable $\mathbf{y}(s)$ on the right hand side of Eq. (3.2). Eq. (3.1) shows that the unit tangent vector $\dot{\mathbf{y}}(s)$ belongs to the null space of $DH(\mathbf{y}(s))$, and is uniquely determined. Therefore, the solution manifolds we wish to follow are one-dimensional solution curves. In order to fit the physical property of the two-component BEC, we split the unit tangent vector $\dot{\mathbf{y}}=(\dot{\alpha},\dot{\beta},\dot{\tilde{\alpha}},\dot{\tilde{\beta}},\dot{\lambda}_1,\dot{\lambda}_2)^T\in\mathbf{R}^{(4N^2+2)}$ into $\dot{\mathbf{y}}=\dot{\mathbf{y}}_1+\dot{\mathbf{y}}_2$, with $\dot{\mathbf{y}}_1=(\dot{\alpha},\dot{\beta},0,0,\dot{\lambda}_1,0)^T$ and $\dot{\mathbf{y}}_2=(0,0,\dot{\tilde{\alpha}},\dot{\tilde{\beta}},0,\dot{\lambda}_2)^T$, and normalize $\dot{\mathbf{y}}_1$ and $\dot{\mathbf{y}}_2$ such that $\|\dot{\mathbf{y}}_1\|_2=\|\dot{\mathbf{y}}_2\|_2=1$. Note that the augmented Jacobian matrix

$$A(\mathbf{y}(s))=\begin{bmatrix} DH(\mathbf{y}(s)) \\ \dot{\mathbf{y}}_1^T(s) \\ \dot{\mathbf{y}}_2^T(s) \end{bmatrix}\in\mathbf{R}^{(4N^2+2)\times(4N^2+2)} \tag{3.3}$$

is nonsingular for all $s\in I$, except at primary bifurcation points on the trivial solution curve $\{(0,0,0,0,\lambda_1,\lambda_2)|\lambda_1,\lambda_2\in\mathbf{R}\}$ where the Jacobian matrix $DH(\mathbf{y}(s))$ has rank deficiency. Thus, to switch from the trivial solution curve to the primary solution branch near the bifurcation point, we solve the perturbed nonlinear system

$$H(\mathbf{x},\Lambda)+\mathbf{d}=0$$

for some perturbation vector $\mathbf{d}\in\mathbf{R}^{4N^2}$.

https://doi.org/10.4208/cicp.151214.021015a Published online by Cambridge University Press

In the first step of the continuation method we compute the first approximating point, say $(u_1^{(0)},v_1^{(0)},u_2^{(0)},v_2^{(0)},\lambda_1^{(0)},\lambda_2^{(0)})=(0,0,0,0,\lambda_1^{(0)},\lambda_2^{(0)})$ of Eq. (2.4) with $\tilde{U}(u_j,v_j)=\tilde{\Phi}(u_j,v_j)=0, j=1,2$. Next, we compute $\tilde{U}(u_j^{(0)},v_j^{(0)}),\tilde{\Phi}(u_j^{(0)},v_j^{(0)}), j=1,2$, and plug these two terms into Eq. (2.4). In general, let

$$\begin{aligned}\mathbf{y}^{(k)} &= (u_1^{(k)},v_1^{(k)},u_2^{(k)},v_2^{(k)},\lambda_1^{(k)},\lambda_2^{(k)})\\ &= \Big(\textstyle\sum_{i,j=1}^N \alpha_{ij}^{(k)}\sin i\pi x\sin j\pi y,\sum_{i,j=1}^N \beta_{ij}^{(k)}\sin i\pi x\sin j\pi y,\\ &\quad \textstyle\sum_{i,j=1}^N \tilde{\alpha}_{ij}^{(k)}\sin i\pi x\sin j\pi y,\sum_{i,j=1}^N \tilde{\beta}_{ij}^{(k)}\sin i\pi x\sin j\pi y,\lambda_1^{(k)},\lambda_2^{(k)}\Big)\\ &\in \mathbf{R}^{4N^2+2}\end{aligned}$$

be the approximating point for the solution curve c obtained by the k^{th} step continuation method. A new point $\mathbf{y}_{(1)}^{(k+1)}$ is predicted by the Euler predictor or the pseudo-arclength predictor [18]

$$\mathbf{y}_{(1)}^{(k+1)}=\mathbf{y}^{(k)}+\delta^{(k)}\cdot\dot{\mathbf{y}}^{(k)},$$

where $\delta^{(k)}>0$ is the step length, and $\dot{\mathbf{y}}^{(k)}=(\dot{\alpha}^{(k)},\dot{\beta}^{(k)},\dot{\tilde{\alpha}}^{(k)},\dot{\tilde{\beta}}^{(k)},\dot{\lambda}_1^{(k)},\dot{\lambda}_2^{(k)})$ is the unit tangent vector at $\mathbf{y}^{(k)}$ which is obtained by solving the linear system

$$\begin{bmatrix} DH(\mathbf{y}^{(k)}(s)) \\ (\dot{\mathbf{y}}_1^{(k-1)}(s))^T \\ (\dot{\mathbf{y}}_2^{(k-1)}(s))^T \end{bmatrix}\cdot\dot{\mathbf{y}}^{(k)}=\begin{bmatrix}\bar{0}\\1\\1\end{bmatrix},\quad \text{where } \bar{0}\in\mathbf{R}^{4N^2}. \tag{3.4}$$

Note that the Euler predictor can be replaced by higher order predictors such as the Taylor predictors. In the Newton corrector, we solve the linear system

$$\begin{bmatrix} DH(\mathbf{y}_{(l)}^{(k+1)}(s)) \\ (\dot{\mathbf{y}}_1^{(k)}(s))^T \\ (\dot{\mathbf{y}}_2^{(k)}(s))^T \end{bmatrix}\cdot w_{(l)}=\begin{bmatrix}-H(\mathbf{y}_{(l)}^{(k+1)})\\0\\0\end{bmatrix},\quad l=1,2,\cdots, \tag{3.5}$$

where $\mathbf{y}_{(l+1)}^{(k+1)}=\mathbf{y}_{(l)}^{(k+1)}+w_{(l)}$. We perform the Newton iteration until it converges to the next approximating point $(u_1^{(k+1)}, v_1^{(k+1)}, u_2^{(k+1)},v_2^{(k+1)}, \lambda_1^{(k+1)}, \lambda_2^{(k+1)})$. The continuation algorithm is implemented in this way until the target point $(u_1^*,v_1^*,u_2^*,v_2^*,\lambda_1^*,\lambda_2^*)$ is reached, where $(u_j^*)^2+(v_j^*)^2=1$, $j=1,2$, are the discrete normalization conditions.

We denote the continuation algorithm described above by Algorithm 3.1, which will be used in our numerical experiments for both one-component and binary Rydberg-dressed BEC.

4 Divide-and-conquer with rescaling

The main difficulty of tracing the ground state solution curve of (binary) Rydberg-dressed BEC using a continuation method is that the ranges for the chemical potential $\lambda/\lambda_j, j=1,2$

https://doi.org/10.4208/cicp.151214.021015a Published online by Cambridge University Press

and the coefficients of the nonlocal nonlinear term/terms are quite different in scale. The difficulty is manifest when the contour at some point of the solution branch evolves from one peak to vortices, which will cause the divergence of Newton's method. To overcome the drawback, we rescale the range/ranges of the nonlocal nonlinear term/terms using the divide-and-conquer strategy. This will helps us to choose a proper stepsize for curve tracing. The technique guarantees that the solution branch we wish to follow can be well-approximated.

4.1 One-component BEC

Let μ^* be the maximum value for the coefficient μ in Eq. (1.6). Theoretically we can use both the chemical potential λ and the parameter μ as the two components for the parameter variable. However, the continuation increment with respect to the chemical potential λ, mainly, the stepsize for curve-tracing is relatively small, say, from 10^{-1} to 10^{-2}, depending on the curvature of the solution curve, compared to that of μ. Therefore, it requires large number of continuation steps to trace the solution curve which could be expensive. To overcome the drawback, we impose an additional parameter $\nu\in[0,1]$ on the integral term of Eq. (1.6). That is, we rescale the interval $[0,\mu^*]$ by $[0,\nu^*]$ with $\nu^*=1$ and let $\mu=\nu\mu^*$. And we rewrite Eq. (1.6) as

$$\widetilde{F}(\psi,\lambda,\nu)=\Big[-\frac{1}{2}\Delta+V(\mathbf{r})+\gamma U(\psi)+\nu\mu^*\Phi(\psi)-\omega L_z-\lambda\Big]\psi=0,\quad \nu\in[0,1],\ \ \mathbf{r}\in\Omega,$$
$$\psi(\mathbf{r})=0\ \text{ on }\partial\Omega, \tag{4.1}$$

where

$$U(\psi)=|\psi(\mathbf{r})|^2, \tag{4.2}$$
$$\Phi(\psi)=\int g(\mathbf{r}-\mathbf{r}')|\psi(\mathbf{r}')|^2d\mathbf{r}'=\mathcal{F}^{-1}\big[\mathcal{F}[g(\mathbf{r})]\cdot\mathcal{F}[|\psi(\mathbf{r})|^2]\big]. \tag{4.3}$$

Eq. (4.1) characterizes two important applications of continuation methods, namely, solving nonlinear eigenvalue problems, and the homotopy continuation which connects the GPE without long-range interaction term and with long-range interaction term.

To start with, we set $\nu=\mu=0$, and omit the rotating term. Then we implement the predictor-corrector continuation algorithm with λ as the parameter variable. And we trace the ground state solution of Eq. (4.1) until the normalization condition (1.7) is satisfied, which is the target point of the first step curve-tracing. Next, we implement the continuation algorithm with the chemical potential λ and the parameter ν as the components of the parameter variable, where the last unit tangent vector obtained in the predictor-corrector continuation algorithm, and the normalization condition (1.7) are used as the two constraint vectors for bordered linear systems. For the case $\omega=0$ and $0<\nu<\tilde{\nu}<1$ for some $\tilde{\nu}$, the contours of the ground state solution branch consists of one peak with ring structure. When the contour starts to evolve from one peak with ring structure to a

https://doi.org/10.4208/cicp.151214.021015a Published online by Cambridge University Press

hexagonal crystal structure, the divide-and-conquer technique is necessary for rescaling the range of the nonlocal nonlinear term. Otherwise Newton's method would diverge. The implementation for the case $\omega\in(0,1)$ is exactly the same as that for the case $\omega=0$. We observe that the solution curve has a big jump (see Fig. 3) when the contour of the ground state solution starts to evolve from one peak to vortices which is affected by the rotating term. If the stepsize is too small, then the contour of the solution with one peak will never evolve to vortices. On the other hand, if the stepsize is too large, then Newton's method will diverge. In order to obtain numerical results with physical meaning, the solution branch has to be well-approximated.

Algorithm 4.1. A pseudo-arclength continuation algorithm for one-component Rydberg-dressed BEC.

Initialization: Choose $\gamma=\gamma_0$, $\mu=\mu^*$, $\omega=\omega_0$, $\nu=0$.

Step 1. Implement the predictor-corrector continuation algorithm with λ as the parameter variable to trace the first solution curve of Eq. (4.1) until the normalization condition (1.7) is satisfied.

Step 2. Implement the pseudo-arclength continuation algorithm to trace the first solution curve of Eq. (4.1) with $\Lambda=(\lambda,\nu)$, until $\nu=1$ is reached.

4.2 Two-component BEC

For two-component BEC we have two constraint conditions, namely, the normalization conditions (1.5), in addition to the splitting of the tangent vector given in Section 3. We will describe a pseudo-arclength continuation algorithm, where the parameter variable $\Lambda\in\mathbf{R}^4$. Let μ_0^* and μ_1^* be the maximum values for the coefficients $\mu_{12}=\mu_{21}$ and $\mu_{11}=\mu_{22}$, respectively. We rescale the intervals $[0,\mu_0^*]$ and $[0,\mu_1^*]$ by the intervals $[0,\nu_0^*]$ and $[0,\nu_1^*]$, respectively, where $\nu_0^*\le\mu_0^*$ and $\nu_1^*\le\mu_1^*$. In addition, let $\mu_0=\mu_0^*/\nu_0^*$ and $\mu_1=\mu_1^*/\nu_1^*$, and define $\mu_{12}=\mu_{21}=\nu_0\mu_0\in[0,\mu_0^*]$, $\mu_{11}=\mu_{22}=\nu_1\mu_1\in[0,\mu_1^*]$, where $\nu_0\in[0,\nu_0^*]$, $\nu_1\in[0,\nu_1^*]$. We rewrite Eq. (2.4) as follows:

$$\begin{aligned}
\widehat{H}_1(u,\Lambda)=&\Big[-\frac{1}{2}\Delta+V(\mathbf{r})+\gamma_{11}\tilde{U}(u_1,v_1)+\gamma_{12}\tilde{U}(u_2,v_2)+\nu_1\mu_1\tilde{\Phi}(u_1,v_1)\\
&+\nu_0\mu_0\tilde{\Phi}(u_2,v_2)-\lambda_1\Big]u_1-\omega(x(v_1)_y-y(v_1)_x)=0,\\
\widehat{H}_2(u,\Lambda)=&\Big[-\frac{1}{2}\Delta+V(\mathbf{r})+\gamma_{11}\tilde{U}(u_1,v_1)+\gamma_{12}\tilde{U}(u_2,v_2)+\nu_1\mu_1\tilde{\Phi}(u_1,v_1)\\
&+\nu_0\mu_0\tilde{\Phi}(u_2,v_2)-\lambda_1\Big]v_1+\omega(x(u_1)_y-y(u_1)_x)=0,\\
\widehat{H}_3(u,\Lambda)=&\Big[-\frac{1}{2}\Delta+V(\mathbf{r})+\gamma_{22}\tilde{U}(u_2,v_2)+\gamma_{21}\tilde{U}(u_1,v_1)+\nu_1\mu_1\tilde{\Phi}(u_2,v_2)\\
&+\nu_0\mu_0\tilde{\Phi}(u_1,v_1)-\lambda_2\Big]u_2-\omega(x(v_2)_y-y(v_2)_x)=0,
\end{aligned}$$

https://doi.org/10.4208/cicp.151214.021015a Published online by Cambridge University Press

$$\widehat{H}_4(u,\Lambda)=\Big[-\frac{1}{2}\Delta+V(\mathbf{r})+\gamma_{22}\tilde{U}(u_2,v_2)+\gamma_{21}\tilde{U}(u_1,v_1)+\nu_1\mu_1\tilde{\Phi}(u_2,v_2)$$
$$+\nu_0\mu_0\tilde{\Phi}(u_1,v_1)-\lambda_2\Big]v_2+\omega(x(u_2)_y-y(u_2)_x)=0,$$
$$\nu_0\in[0,\nu_0^*],\ \nu_1\in[0,\nu_1^*],\ \mathbf{r}\in\Omega=(-l,l)^2,\ \psi_j(\mathbf{r})=0\ \text{ on }\partial\Omega,\ j=1,2, \tag{4.4}$$

where $u=(u_1,v_1,u_2,v_2)$, and $\Lambda=(\lambda_1,\lambda_2,\nu_0,\nu_1)$. Besides, the two normalization conditions in Eq. (1.5) are imposed as the two constraint vectors for the bordered linear systems, and are denoted by

$$\widehat{H}_5(u,\Lambda)=0,\quad \widehat{H}_6(u,\Lambda)=0, \tag{4.5}$$

where $\widehat{H}_5$ and $\widehat{H}_6$ correspond to $(u_1^2+v_1^2)-1$ and $(u_2^2+v_2^2)-1$, respectively. Note that the parameters λ_1,λ_2, ν_0 and ν_1 have different ranges.

First, we set $\nu_0=\nu_1=0$, i.e., $\mu_{11}=\mu_{22}=\mu_{12}=\mu_{21}=0$, and implement Algorithm 3.1 with $\Lambda=(\lambda_1,\lambda_2)\in\mathbf{R}^2$. We trace the ground state solution curve until the normalization conditions (1.5) are satisfied. Next, we use the chemical potentials λ_1,λ_2 together with the parameter ν_0,ν_1 as the four components of the parameter variable Λ, and implement the pseudo-arclength continuation algorithm. Here the splitting of the last unit tangent vector obtained in Algorithm 3.1, and the normalization conditions (1.5) are used as the four constraint vectors for the bordered linear systems. The associated nonlinear system of equations is given by

$$\widehat{H}(\mathbf{x},\Lambda)=\big[\widehat{H}_1,\widehat{H}_2,\widehat{H}_3,\widehat{H}_4,\widehat{H}_5,\widehat{H}_6\big]^T=\bar{0}, \tag{4.6}$$

where $\mathbf{x}=(\alpha,\beta,\tilde{\alpha},\tilde{\beta})$, and $\Lambda=(\lambda_1,\lambda_2,\nu_0,\nu_1)$. Denote the Jacobian matrix of $\widehat{H}$ by $D\widehat{H}\in\mathbf{R}^{(4N^2+2)\times(4N^2+4)}$. To compute the unit tangent vector $\dot{\mathbf{y}}^{(k)}=(\dot{\alpha}^{(k)},\dot{\beta}^{(k)},\dot{\tilde{\alpha}}^{(k)},\dot{\tilde{\beta}}^{(k)},\dot{\lambda}_1^{(k)},\dot{\lambda}_2^{(k)},\dot{\nu}_0^{(k)},\dot{\nu}_1^{(k)})^T\in\mathbf{R}^{(4N^2+4)}$, we solve the linear system

$$\begin{bmatrix} D\widehat{H}(\mathbf{y}^{(k)}) \\ (\dot{\mathbf{y}}_1^{(k-1)})^T \\ (\dot{\mathbf{y}}_2^{(k-1)})^T \end{bmatrix}\dot{\mathbf{y}}^{(k)}=\begin{bmatrix}\bar{0}\\1\\1\end{bmatrix},$$

where $\dot{\mathbf{y}}_1^{(k-1)}+\dot{\mathbf{y}}_2^{(k-1)}=\dot{\mathbf{y}}^{(k-1)}$ is the splitting of the previous unit tangent vector $\dot{\mathbf{y}}^{(k-1)}$, $\dot{\mathbf{y}}_1^{(k-1)}=(\dot{\alpha}^{(k-1)},\dot{\beta}^{(k-1)},0,0,\dot{\lambda}_1^{(k-1)},0,\dot{\nu}_0^{(k-1)},0)^T$, $\dot{\mathbf{y}}_2^{(k-1)}=(0,0,\dot{\tilde{\alpha}}^{(k-1)},\dot{\tilde{\beta}}^{(k-1)},0,\dot{\lambda}_2^{(k-1)},0,\dot{\nu}_1^{(k-1)})^T$, and $\bar{0}\in\mathbf{R}^{4N^2+2}$. In the Newton corrector, we solve the linear system

$$\begin{bmatrix} D\widehat{H}(\mathbf{y}_l^{(k+1)}) \\ (\dot{\mathbf{y}}_1^{(k)})^T \\ (\dot{\mathbf{y}}_2^{(k)})^T \end{bmatrix}w_{(l)}=\begin{bmatrix}-\widehat{H}(\mathbf{y}_{(l)}^{(k+1)})\\0\\0\end{bmatrix},\quad l=1,2,\cdots.$$

We observe that the parameter ν_1 reaches the desired value ν_1^* earlier than that of the parameter ν_0, which shows that the parameters $\mu_{12}=\mu_{21}$ and $\mu_{11}=\mu_{22}$ indeed have different increments. Then we reduce the parameter variable $\Lambda\in\mathbf{R}^4$ to $\Lambda_1=(\lambda_1,\lambda_2,\nu_0)$.

https://doi.org/10.4208/cicp.151214.021015a Published online by Cambridge University Press

Now only three constraint conditions are required. So we use the unit tangent vector $\dot{\mathbf{y}}=(\dot{\alpha},\dot{\beta},\dot{\tilde{\alpha}},\dot{\tilde{\beta}},\dot{\lambda_1},\dot{\lambda_2},\dot{\nu_0})$ together with the normalization conditions (1.5) as the three constraint conditions. The nonlinear system of equations associated with the three-parameter continuation algorithm is given by

$$\widetilde{H}(\mathbf{x},\Lambda_1)=\left[\widetilde{H}_1,\widetilde{H}_2,\widetilde{H}_3,\widetilde{H}_4,\widetilde{H}_5,\widetilde{H}_6\right]^T=\bar{0}. \tag{4.7}$$

Note that $\widehat{H}_j$ and $\widetilde{H}_j$ represent exactly the same equations, $j=1:6$ except that in Eq. (4.7) we treat $\mu_{11}=\mu_{22}$ as a constant, while $\mu_{11}=\mu_{22}=\nu_1\mu_1$ is a variable in Eq. (4.6). Denote the Jacobian matrix of $\widetilde{H}$ by $D\widetilde{H}\in\mathbf{R}^{(4N^2+2)\times(4N^2+3)}$. To compute the unit tangent vector $\dot{\mathbf{y}}^{(k)}=(\dot{\alpha}^{(k)},\dot{\beta}^{(k)},\dot{\tilde{\alpha}}^{(k)},\dot{\tilde{\beta}}^{(k)},\dot{\lambda}_1^{(k)},\dot{\lambda}_2^{(k)},\dot{\nu}_0^{(k)})^T\in\mathbf{R}^{(4N^2+3)}$, we solve the linear system

$$\begin{bmatrix} D\widetilde{H}(\mathbf{y}^{(k)}) \\ (\dot{\mathbf{y}}^{(k-1)})^T \end{bmatrix}\dot{\mathbf{y}}^{(k)}=\begin{bmatrix} \bar{0} \\ 1 \end{bmatrix},\ \text{where } \bar{0}\in\mathbf{R}^{4N^2+2}.$$

A new approximating point is predicted by the Euler predictor

$$\mathbf{y}_{(1)}^{(k+1)}=\mathbf{y}^{(k)}+\delta^{(k)}\cdot\dot{\mathbf{y}}^{(k)},$$

where $\delta^{(k)}>0$ is the step length. The implementation of the Newton corrector is exactly the same as that of the continuation algorithm in [32], and is omitted here. We trace the first solution curve of Eq. (4.7) until the value $\nu_0=\nu_0^*$ is reached. Now the ground state solutions for various values of the coefficient $\mu_{12}=\mu_{21}$ are available on the solution curve.

Algorithm 4.2. A pseudo-arclength continuation for two-component Rydberg-dressed BEC.

Initialization: Choose $\nu_0=0$, $\nu_1=0$.

Step 1. Implement Algorithm 3.1 to trace the first solution curve of Eq. (4.4) until the normalization conditions (1.5) are satisfied.

Step 2. Implement the continuation algorithm with $\Lambda\in\mathbf{R}^4$ to trace the first solution curve of Eq. (4.6), until $\nu_1=\nu_1^*$ is reached.

Step 3. Reduce the four-constraint continuation algorithm to the three-constraint one, where the unit tangent vector and the normalization conditions (1.5) are used as the constraint conditions. Trace the solution branch until $\nu_0=\nu_0^*$ is reached.

Actually, in Algorithm 4.2 we may skip Step 2, and implement Step 3 directly with $\Lambda_1=(\lambda_1,\lambda_2,\nu_0)$, where the coefficients of $\mu_{11}=\mu_{22}=:\mu_1^*$ are fixed. We refer to this special case by Algorithm 4.3, which was implemented in our numerical experiments.

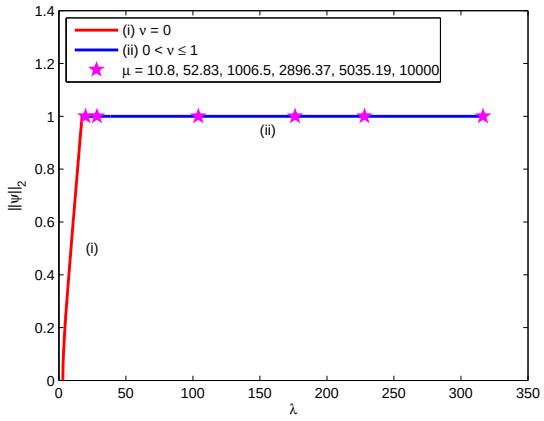
Proposition 4.1. If we choose $\gamma_{11}=\gamma_{22}$, $\gamma_{12}=\gamma_{21}$, $\mu_{11}=\mu_{22}$, and $\mu_{12}=\mu_{21}$ in Eq. (4.4), then we have $\|\psi_1\|_2=\|\psi_2\|_2$ and $\lambda_1=\lambda_2$ throughout the curve-tracing.

Proof. This follows from the definition of $\tilde{\Phi}$ in Equation (2.6), and the fact that the two components ψ_1 and ψ_2 are symmetric with respect to the operator in Eq. (4.4). □

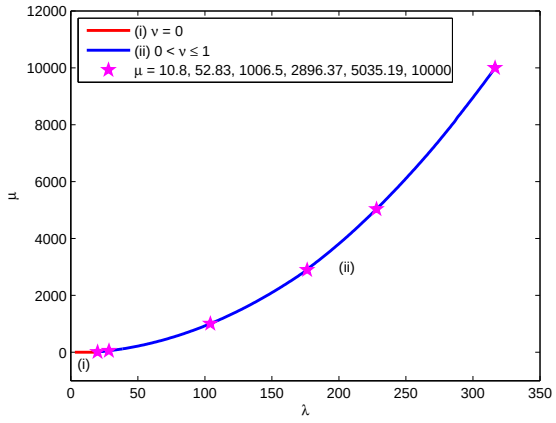
https://doi.org/10.4208/cicp.151214.021015a Published online by Cambridge University Press

5 Numerical results

Example 5.1. Comparison between Algorithms 3.1 and 4.1 for trapped Rydberg-dressed BEC, where the radius frequency $\eta=3$, $\omega=0$, $\gamma=100$, $\mu^*=10000$, $\Omega=(-12,12)^2$, and $N=75$. Algorithm 4.1 was implemented to trace the first solution branch of Eq. (4.1). In Fig. 1(a) the solution curve (i) and (ii) were obtained by implementing Steps 1 and 2 of Algorithm 4.1, respectively. Both represent the ground state solution curve of the GPE under the normalization condition (1.7) for all $\mu\in[0,\mu^*]$. Fig. 1(b) depicts the relationship between the two parameters λ and μ, where the solution curves (i) and (ii) correspond to the counterparts of Fig. 1(a), respectively. Fig. 2 displays the contour plots



(a) The ground state solution curve of Eq. (1.6).



(b) The relationship between λ and μ.

Figure 1: Implementing Algorithm 4.1 for trapped Rydberg-dressed BEC, where η=3, ω=0, γ=100, μ^*=10000, and $\Omega=(-12,12)^2$.

https://doi.org/10.4208/cicp.151214.021015a Published online by Cambridge University Press

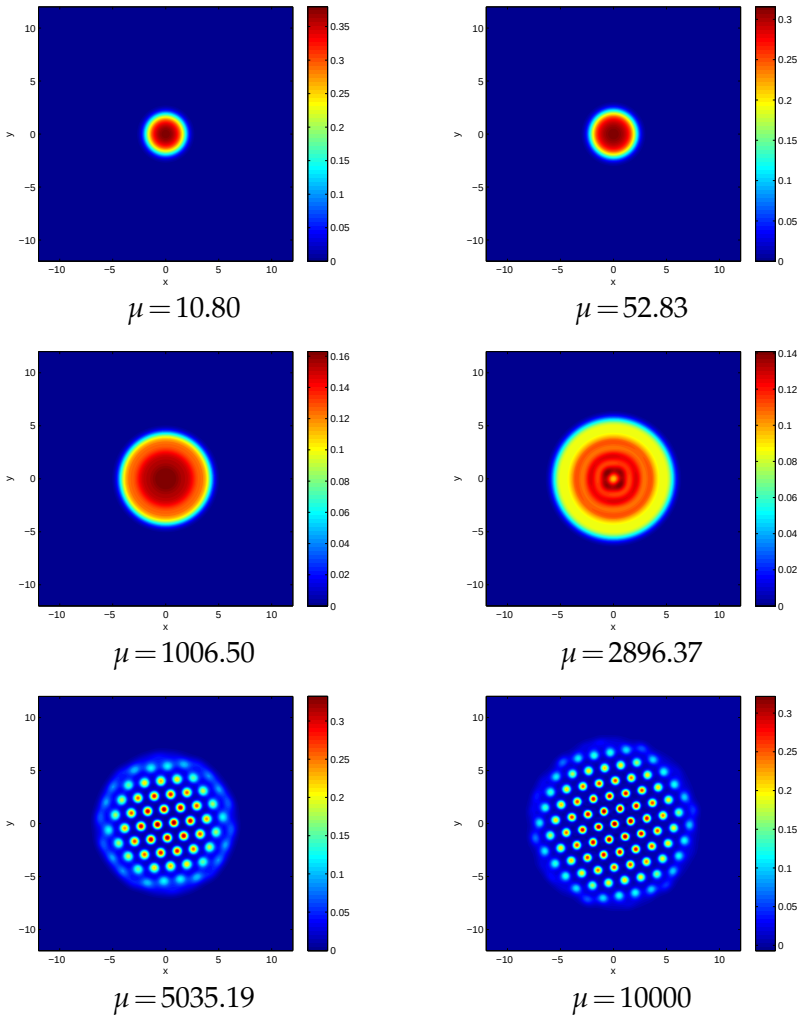
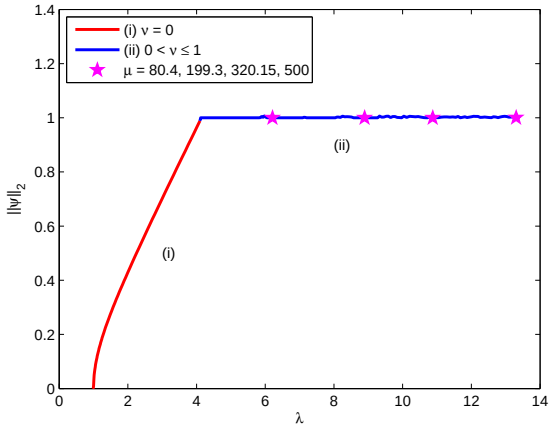


Figure 2: Implementing Algorithm 4.1 for density modulations of Rydberg-dressed BEC where, $\eta = 3$, $\omega = 0$, $\gamma = 100$, and $\mu^* = 10000$. The case $\mu = 2896.37$ corresponds to ring-like structure, while the case $\mu \geq 5035.19$ corresponds to the hexagonal crystal structures of BEC droplets.

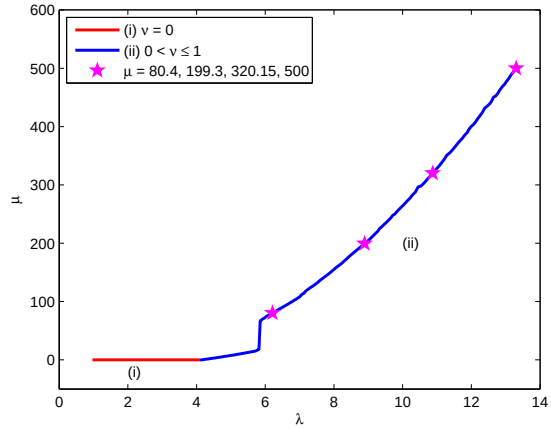
of the ground state solutions, where we picked the μ values from the ground state solution curve (ii) in Fig. 1(a). Next, we implemented Algorithm 3.1 to trace the ground state solution curves of Eq. (4.1), where the μ values were the same as those shown in Fig. 2, namely, $\mu = 10.8, 52.83, 1006.50, 2896.37, 5035.19$, and 10000. Table 1 shows that Algorithm 4.1 outperforms Algorithm 3.1 from the viewpoint of execution time.

Example 5.2. Comparison between Algorithms 3.1 and 4.1 for rotating trapped Rydberg-dressed BEC, where $\eta = 1$, $\omega = 0.85$, $\gamma = 50$, $\mu^* = 500$, $\Omega = (-12,12)^2$, and $N = 59$. First, Algorithm 4.1 was implemented to trace the first solution curve of Eq. (4.1). In Fig. 3(a)

https://doi.org/10.4208/cicp.151214.021015a Published online by Cambridge University Press



(a) The ground state solution curve of Eq. (1.6).



(b) The relationship between λ and μ.

Figure 3: Implementing Algorithm 4.1 for rotating trapped Rydberg-dressed BEC, where $\eta=1$, $\omega=0.85$, $\gamma=50$, $\mu^*=500$, and $\Omega=(-12,12)^2$.

the solution curve (i) and (ii) were obtained by implementing Steps 1 and 2 of Algorithm 4.1, respectively. Both represent the ground state solution curve of the GPE under the normalization condition (1.7) for all $\mu\in[0,\mu^*]$. Fig. 3(b) depicts the relationship between the two parameters λ and μ, where the solution curves (i) and (ii) correspond to the counterparts in Fig. 3(a), respectively. Next, Algorithm 3.1 was implemented to trace the first solution curve of Eq. (4.1) with $\mu=80.40,199.30,320.15,500$. Fig. 4 shows that the contour plots of rotating trapped Rydberg-dressed BEC also have crystalline structure, which form a hexagonal lattice where the peaks in Fig. 2 are replaced by vortices. The execution time listed in Table 2 shows that Algorithm 4.1 is much more efficient than Algorithm 3.1.

https://doi.org/10.4208/cicp.151214.021015a Published online by Cambridge University Press

Table 1: Comparison of the execution time between Algorithms 3.1 and 4.1, where $\eta=3$, $\omega=0$, $\gamma=100$, $\Omega=(-12,12)^2$.

μ	Algorithm 3.1	Algorithm 4.1
10.80	4969.20	-
52.83	5678.74	-
1006.50	10788.09	-
2896.37	23222.17	-
5035.19	34330.60	-
10000	105666.14	-
Total time (sec.)	184654.94	77547.74

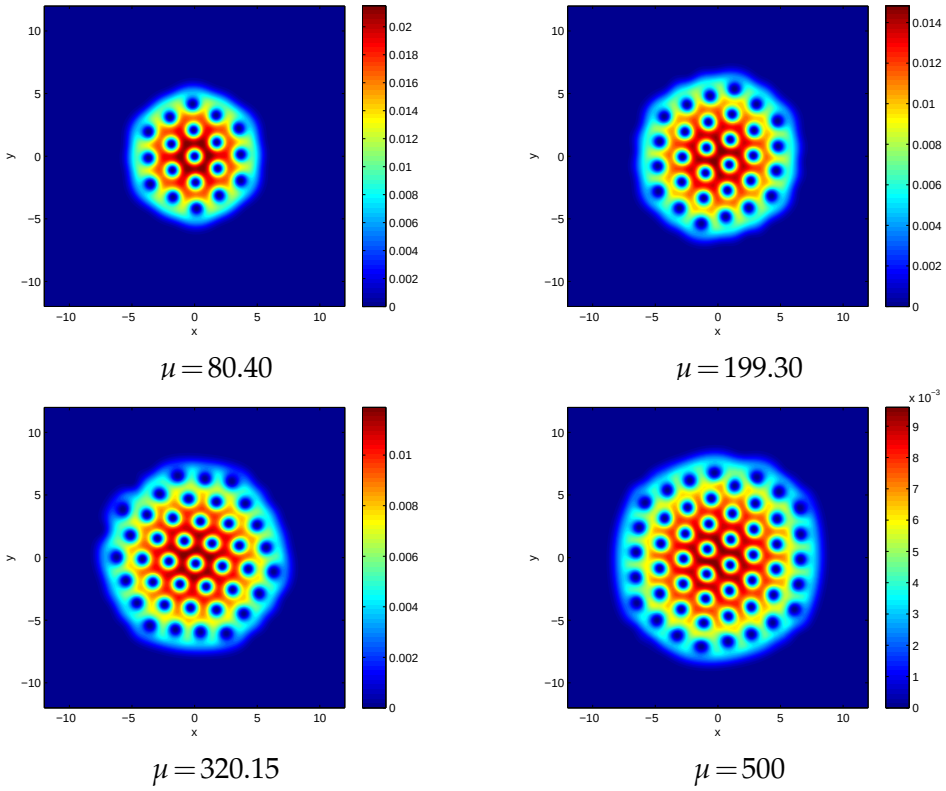
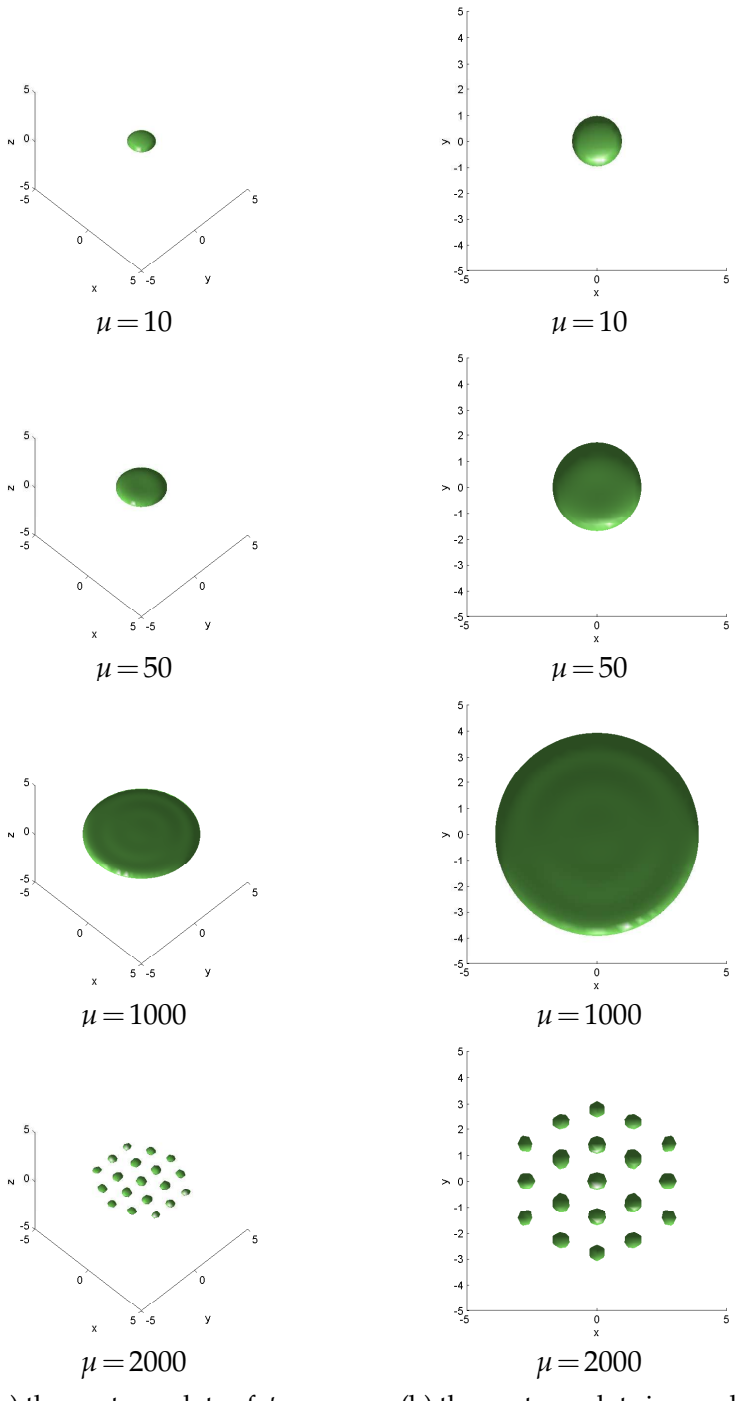


Figure 4: Implementing Algorithms 4.1 for contour plots of rotating trapped Rydberg-dressed BEC with $\eta=1$, $\omega=0.85$, $\gamma=50$, $\mu^*=500$, and $\Omega=(-12,12)^2$.

Example 5.3. Numerical result for 3D trapped Rydberg-dressed BEC, where $\eta=3$, $\omega=0$, $\gamma=0$, $\mu^*=2000$, $\Omega=(-5,5)^3$, and $N=21$. Fig. 5 shows that the contour plots of 3D trapped Rydberg-dressed BEC forms a hexagonal lattice.

https://doi.org/10.4208/cicp.151214.021015a Published online by Cambridge University Press



(a) the contour plots of ψ (b) the contour plots in xy-plane

Figure 5: Density modulation of 3D trapped Rydberg-dressed BEC, where $\eta=3$, $\omega=0$, $\gamma=0$, $\mu=10$, 50, 1000, 2000, and $\Omega=(-5,5)^3$. The case $\mu=2000$ corresponds to the hexagonal crystal structures of BEC droplets.

https://doi.org/10.4208/cicp.151214.021015a Published online by Cambridge University Press

Table 2: Comparison of the execution time between Algorithms 3.1 and 4.1, where $\eta=1$, $\omega=0.85$, $\gamma=50$, $\Omega=(-12,12)^2$.

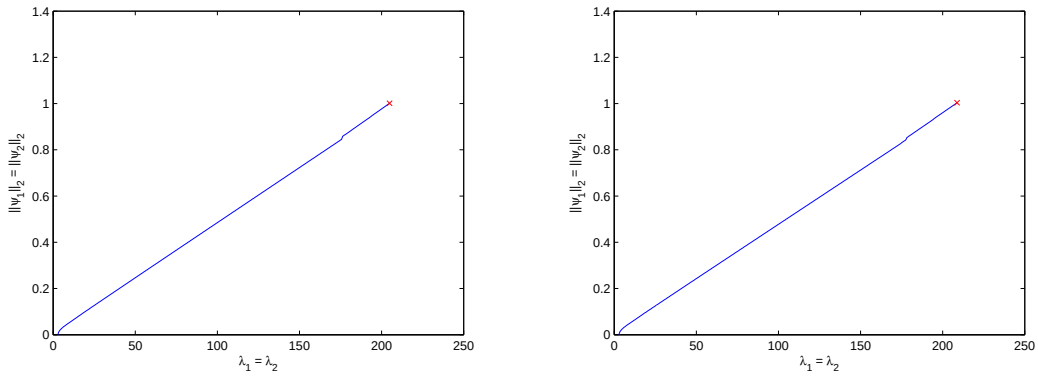
μ	Algorithm 3.1	Algorithm 4.1
80.40	6948.15	-
199.30	11257.02	-
320.15	14523.35	-
500	18108.29	-
Total time (sec.)	50836.81	17782.25

Example 5.4. Comparison among Algorithms 3.1, 4.2 and 4.3 for tracing the ground state solutions of Eq. (1.4) without rotating term, where $\eta=3$, $\gamma_{11}=\gamma_{22}=80$, $\gamma_{12}=\gamma_{21}=60$, $\mu_0^*=1000$, $\mu_1^*=4000$, $\mu_{12}=\mu_{21}$ = 25, 150, 450, 1000, $\Omega=(-10,10)^2$, and $N=59$. We traced the ground state solution curves of Eq. (1.4) four times when Algorithm 3.1 was implemented. Fig. 6 shows the ground state solution curves for $\mu_{12}=\mu_{21}$ = 25, 150, 450, and 1000. The result of Fig. 6 shows that the chemical potentials of the system increase with respect to the values of $\mu_{12}=\mu_{21}$. Fig. 7 shows that the density modulations of the wave functions ψ_1 and ψ_2 are almost identical, which form a hexagonal lattice for various values of $\mu_{12}=\mu_{21}$, and verifies the prediction of Proposition 4.1. However, there is a slight rotation between ψ_1 and ψ_2.

Next, Algorithm 4.2 was implemented to trace the ground state solutions, where we did not rescale the interval $[0,\mu_0^*]$, i.e., $[0,\mu_0^*]=[0,\nu_0^*]=[0,1000]$, and rescaled the interval $[0,\mu_1^*]=[0,4000]$ by $[0,\nu_1^*]=[0,10]$. Fig. 8(a) displays the ground state solution curve, where in (i) we did not evaluate all integral terms of the GPE; in (ii) we controlled the increments of the two parameters ν_0 and ν_1 with the same scale; and in (iii) we obtained $\nu_1=10$ or equivalently, $\mu_1^*=4000$. Under this constraint, we computed the contours for various values of ν_0, or $\mu_{12}=\mu_{21}$. Fig. 8(b) shows the relationship between the chemical potentials $\lambda_1=\lambda_2=\lambda$ and the parameters $\mu_{12}=\mu_{21}$, where part (i), (ii), and (iii) correspond to the solution curves (i), (ii), and (iii) in Fig. 8(a). Figs. 8(c) and 8(d) display the relationship between λ and $\mu_{11}=\mu_{22}$, and between $\mu_{12}=\mu_{21}$ and $\mu_{11}=\mu_{22}$, respectively. In order to distinguish the differences of the configurations for the wave functions ψ_1 and ψ_2, we plotted the charge $n:=|\psi_1|^2+|\psi_2|^2$ and the pseudospin $\sigma:=|\psi_1|^2-|\psi_2|^2$ as Hsueh *et al.* did in [33]. Fig. 9 shows the four cases of the charge n and the pseudospin σ which are the same as those obtained in [33] : (i) $\mu_{12}=\mu_{21}=24.05$, honeycomb lattice where one droplet is surrounded by three diverse ones; (ii) $\mu_{12}=\mu_{21}=151.45$, rectangular lattice where one droplet is surrounded by four diverse one; (iii) $\mu_{12}=\mu_{21}=455.74$, triangular lattice with dimeric basis; (vi) $\mu_{12}=\mu_{21}=1000$, triangular lattice without dimeric lattice. Note that we did not show the case (v) in [33] because it represents the domain structure which depends on the size of the domain.

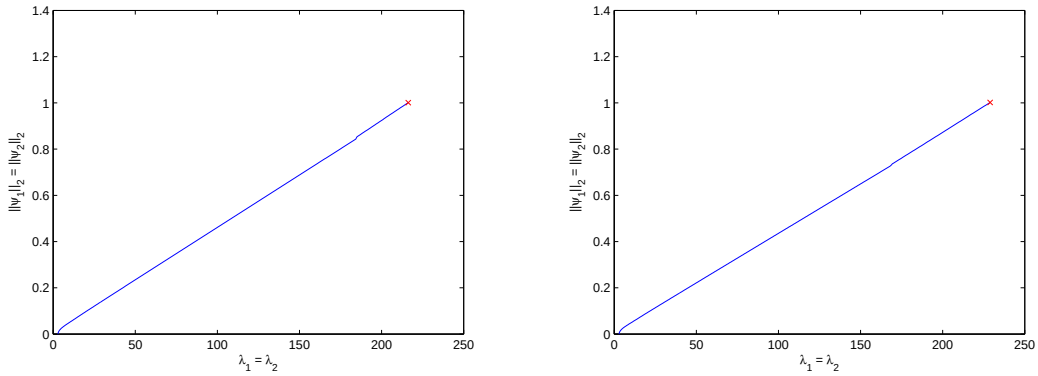
Finally, Algorithm 4.3 was implemented to trace the ground state solution curve of Eq. (1.4), where we rescaled $[0,\mu_0^*]=[0,1000]$ by $[0,\nu_0^*]=[0,10]$. The ground state solution

https://doi.org/10.4208/cicp.151214.021015a Published online by Cambridge University Press



$\lambda_1^* = \lambda_2^* = 204.89849$
$\mu_{12} = \mu_{21} = 25$

$\lambda_1^* = \lambda_2^* = 208.82287$
$\mu_{12} = \mu_{21} = 150$



$\lambda_1^* = \lambda_2^* = 216.26877$
$\mu_{12} = \mu_{21} = 450$

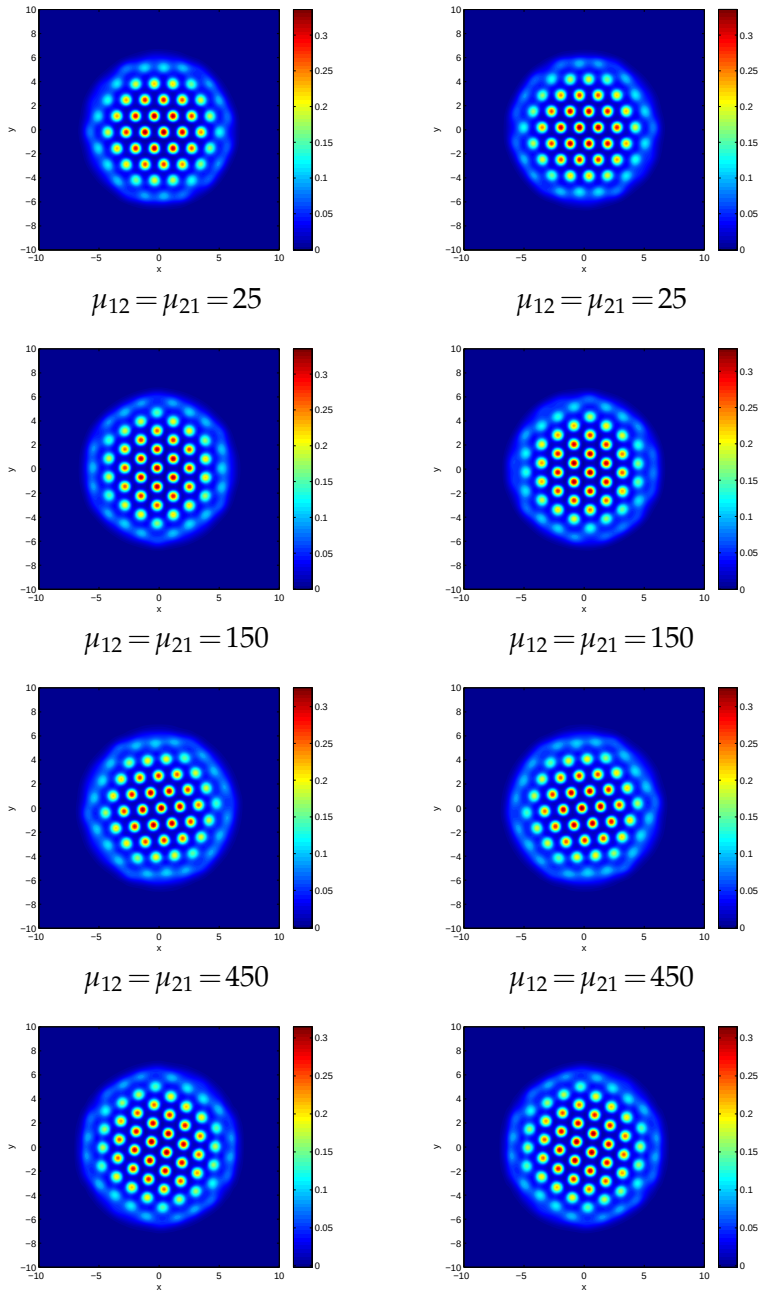
$\lambda_1^* = \lambda_2^* = 228.90467$
$\mu_{12} = \mu_{21} = 1000$

Figure 6: Implementing Algorithm 3.1 for the ground state solution curves in Example 5.4, where $\eta = 3$, $\omega = 0$, $\gamma_{11} = \gamma_{22} = 80$, $\gamma_{12} = \gamma_{21} = 60$, $\mu_{11} = \mu_{22} = 4000$, and $\Omega = (-10,10)^2$.

curve displayed in Fig. 10(a) consists of the solution curves (i) and (ii). In (i) we did not compute the integral terms with coefficients $\mu_{12} = \mu_{21}$. When $\nu_0 > 0$, the solution curve is represented by (ii). Fig. 10(b) shows the relationship between $\lambda = \lambda_1 = \lambda_2$ and $\mu_{12} = \mu_{21}$, where the solution curves (i) and (ii) correspond to the solution curves (i) and (ii) displayed in Fig. 10(a). Fig. 11 shows the contours of the charge n and pseudospin σ. These contours can be obtained from those shown in Fig. 9 via a rotation. Note that the contours of the charge n and pseudospin σ obtained using Algorithm 3.1 also have the same phenomena and are not shown here.

The numerical results listed in Table 3 show that Algorithms 4.2 and 4.3 are more efficient than Algorithm 3.1. Moreover, Algorithm 4.2 outperforms Algorithm 4.3.

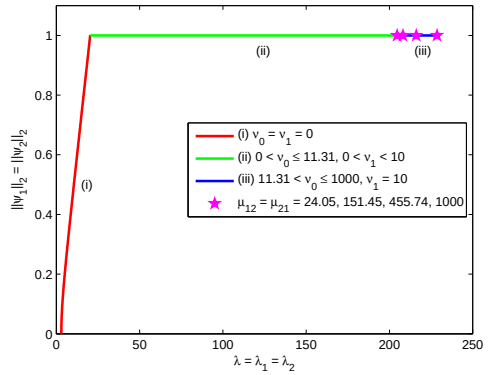
https://doi.org/10.4208/cicp.151214.021015a Published online by Cambridge University Press



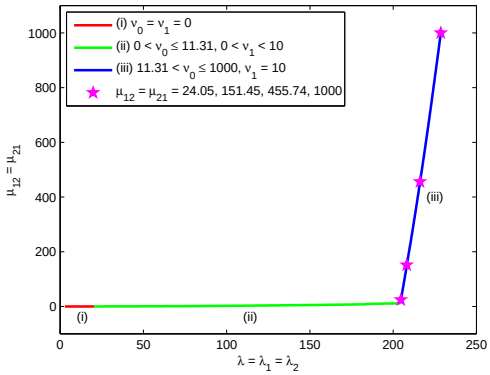
(a) the contour of ψ_1 (b) the contour of ψ_2

Figure 7: Density modulations ψ_1 (left) and ψ_2 (right) of the ground state solutions of binary Rydberg-dressed BEC with $\mu_{12}=\mu_{21}=25$, 150, 450, 1000.

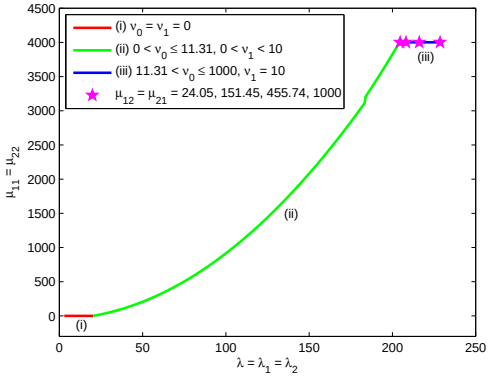
https://doi.org/10.4208/cicp.151214.021015a Published online by Cambridge University Press



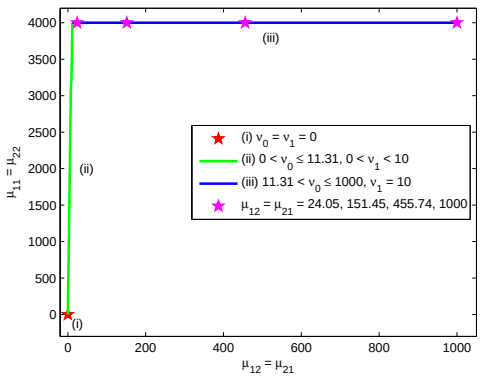
(a) The ground state solution curve of Eq. (1.4).



(b) The relationship between λ and $\mu_{12}=\mu_{21}$.



(c) The relationship between λ and $\mu_{11}=\mu_{22}$.



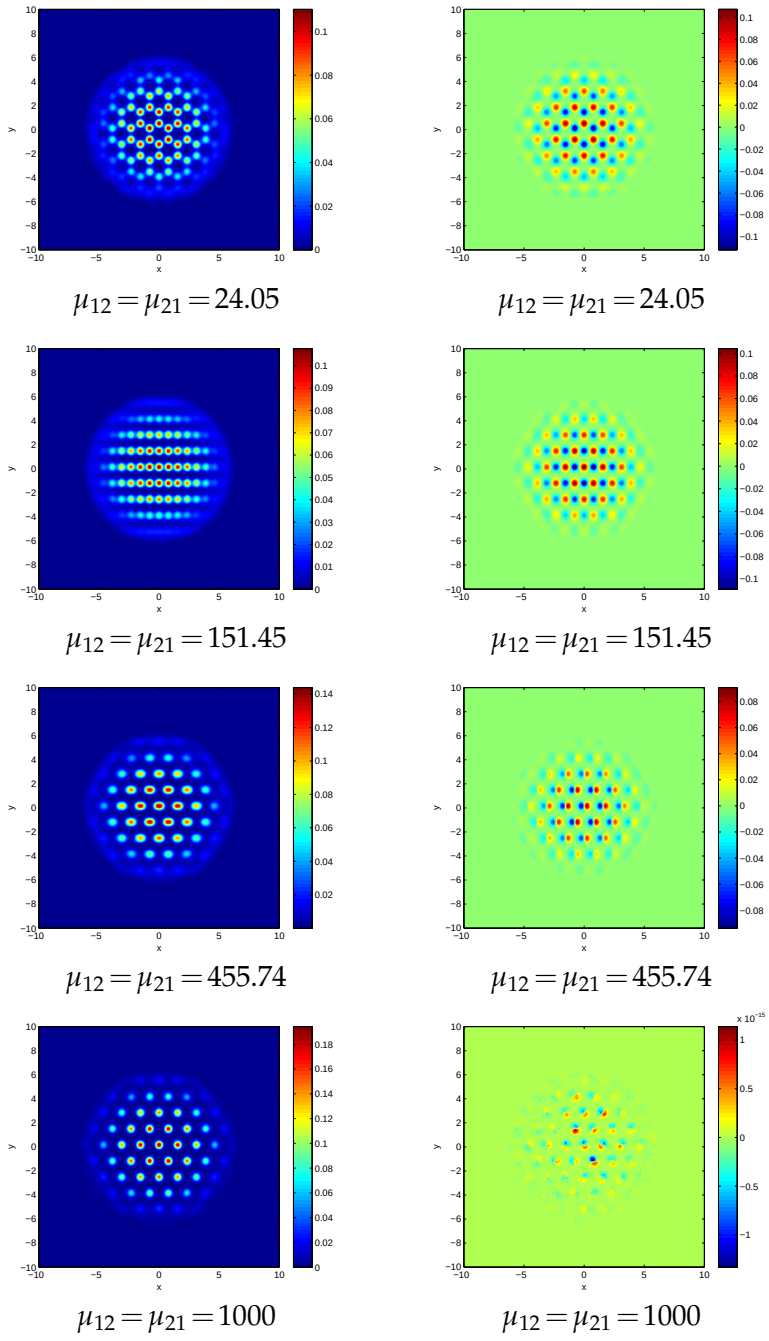
(d) The relationship between $\mu_{12}=\mu_{21}$ and $\mu_{11}=\mu_{22}$.

Figure 8: Implementing Algorithm 4.2 for the ground state solution curve in Example 5.4, where $\eta=3$, $\omega=0$, $\gamma_{11}=\gamma_{22}=80$, $\gamma_{12}=\gamma_{21}=60$, $\mu_0^*=1000$, $\mu_1^*=4000$, $\nu_0^*=1000$, $\nu_1^*=10$, and $\Omega=(-10,10)^2$.

Table 3: Comparison of the execution time among Algorithms 3.1, 4.2 and 4.3, where $\eta=3$, $\omega=0$, $\gamma_{11}=\gamma_{22}=80$, $\gamma_{12}=\gamma_{21}=60$, $\mu_{11}=\mu_{22}=4000$, $\Omega=(-10,10)^2$.

$\mu_{12}=\mu_{21}$	Algorithm 3.1	Algorithm 4.2	Algorithm 4.3
25	43943.57	-	-
150	64349.96	-	-
450	51212.36	-	-
1000	39129.21	-	-
Total time (sec.)	198635.10	54684.45	59268.58

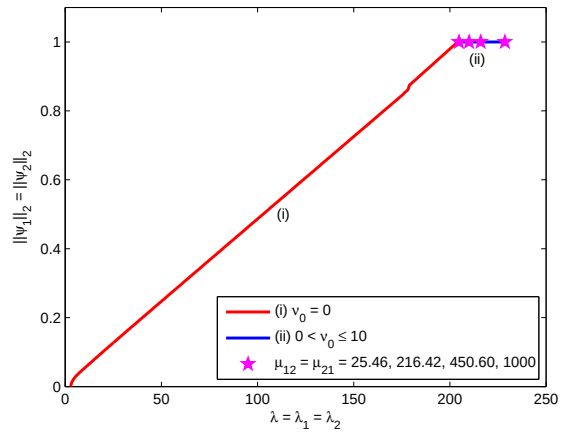
https://doi.org/10.4208/cicp.151214.021015a Published online by Cambridge University Press



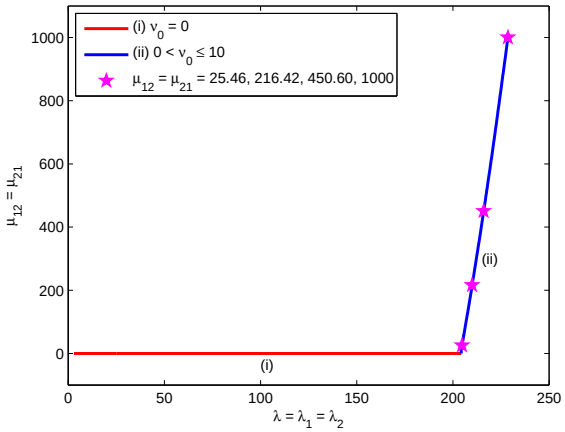
(a) the contour of charge n (b) the contour of pseudospin σ

Figure 9: Implementing Algorithm 4.2 for the ground state solution in Example 5.4, (a) the contour of the charge n, (b) the contour of pseudospin σ, where $\eta=3$, $\omega=0$, $\gamma_{11}=\gamma_{22}=80$, $\gamma_{12}=\gamma_{21}=60$, $\mu_0^*=1000$, $\mu_1^*=4000$, and $\Omega=(-10,10)^2$.

https://doi.org/10.4208/cicp.151214.021015a Published online by Cambridge University Press



(a) The ground state solution curve of Eq. (1.4).



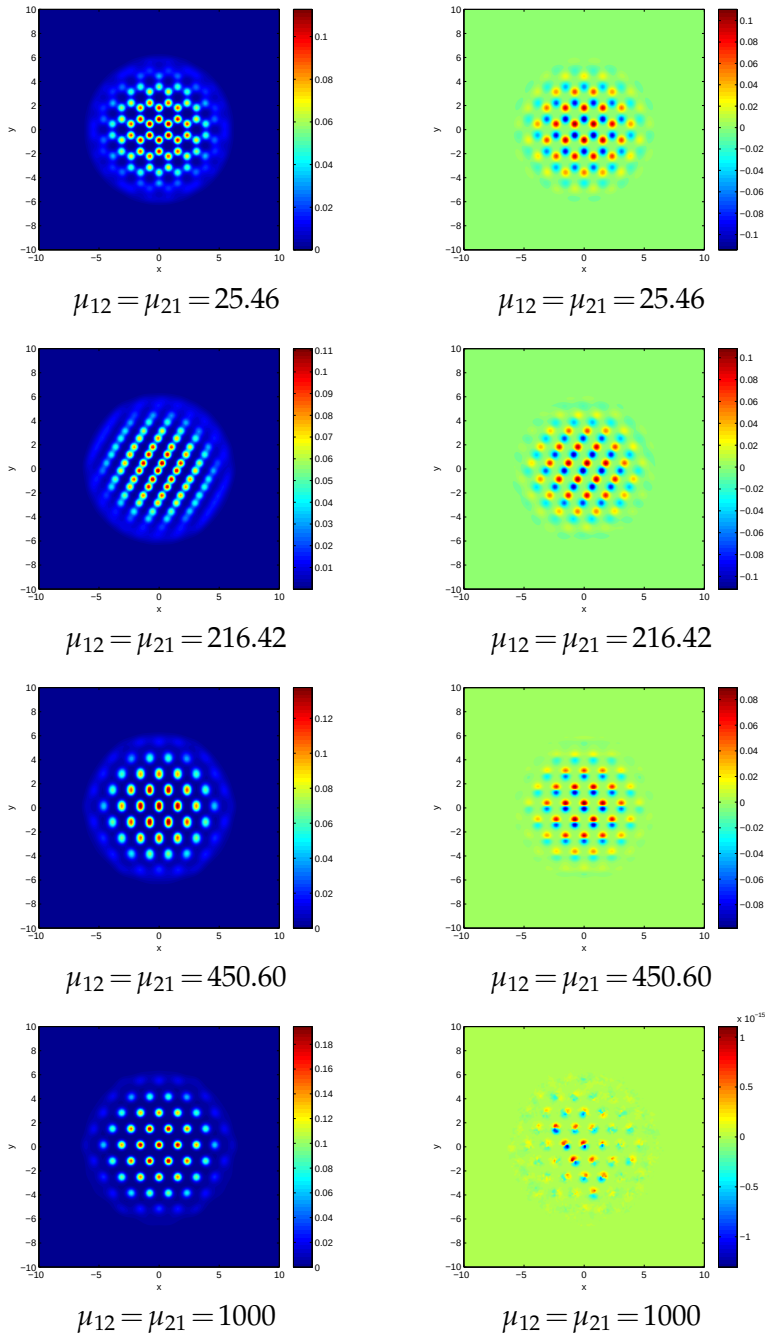
(b) The relationship between λ and $\mu_{12}=\mu_{21}$.

Figure 10: Implementing Algorithm 4.3 for the ground state solution curve in Example 5.4, where $\eta=3$, $\omega=0$, $\gamma_{11}=\gamma_{22}=80$, $\gamma_{12}=\gamma_{21}=60$, $\mu_0^*=1000$, $\mu_1^*=4000$, $\nu_0^*=10$, and $\Omega=(-10,10)^2$.

6 Analysis of numerical results and conclusions

We have proposed some pseudo-arclength continuation algorithms for both (rotating) Rydberg-dressed BEC in 2D and 3D, and binary Rydberg-dressed BEC in 2D. The proposed algorithms have the advantage of tracing the ground state solution curve of the GPE/GPEs once to obtain all configurations of the wave functions for various values of the parameters of the integral terms. On the other hand, when Algorithm 3.1 was implemented we need to trace the first solution curves of Eqs. (1.6) and (1.4) case by case depending on how many ground state solutions we wish to compute for different values

https://doi.org/10.4208/cicp.151214.021015a Published online by Cambridge University Press



(a) the contour of charge n (b) the contour of pseudospin σ

Figure 11: Implementing Algorithm 4.3 for the ground state solution in Example 5.4, (a) the contour of the charge n, (b) the contour of pseudospin σ, where $\eta=3$, $\omega=0$, $\gamma_{11}=\gamma_{22}=80$, $\gamma_{12}=\gamma_{21}=60$, $\mu_0^*=1000$, $\mu_1^*=4000$, and $\Omega=(-10,10)^2$.

https://doi.org/10.4208/cicp.151214.021015a Published online by Cambridge University Press

of $\mu/\mu_{i,j}$, $i,j=1,2$, $i\neq j$. The results of Tables 1–3 show that proposed algorithms with parameter variables in $\mathbf{R}^n, n\geq 2$, are more efficient than Algorithm 3.1.

Based on the numerical results reported in Section 5, we wish to give some concluding remarks concerning the performance of these multiscale algorithms.

(i) We have provided different scales for the parameter(s) of the integral term(s) of Eqs. (1.4) and (1.6). The rescaled parameter(s) have been used as the second, the third and fourth component of the parameter variables for Eqs. (1.6) and (1.4)), respectively. The proposed algorithms can efficiently compute the ground state solutions of Rydberg-dressed BEC and binary Rydberg-dressed BEC.

(ii) Example 5.1 shows that the crystalline structure forms a hexagonal lattice when the number of ground state atoms is large enough. Moreover, the number of droplet lattices increases with respect to the number of ground state atoms. Thus, our results are consistent with those reported in [5].

(iii) Fig. 6 shows that the shapes of the solution curves are almost independent on the number of ground state atoms. However, it requires greater chemical potential for larger number of atoms to form the hexagonal lattice.

(iv) In Example 5.4 we have chosen $\gamma_{11}=\gamma_{22}$, $\gamma_{12}=\gamma_{21}$ for the nonlinear cubic terms, and $\mu_{12}=\mu_{21}$, $\mu_{11}=\mu_{22}$ for the integral terms. Thus the solution curves for the wave functions ψ_1 and ψ_2 are identical. If one of the four pairs of coefficient were chosen to be distinct, it was expected that the two solution curves for ψ_1 and ψ_2 would be separate. In addition, the solution curve corresponding to one component with greater coefficients would satisfy the normalization condition earlier than the other. At any rate, we can make the two components satisfy the normalization conditions at the next continuation step.

Finally, we conclude that the proposed pseudo-arclength continuation algorithms can be applied to solve a system of nonlinear eigenvalue problems with multi-parameters, where the components of the parameter variable have different ranges.

Acknowledgments

We are appreciative to Dr. C.-H. Hsueh of Department of Physics, National Taiwan Normal University for directing us this topic. This work was supported by the Ministry of Science and Technology, Taiwan (R.O.C.) through Project MOST 103-2115-M-231-001-MY2. We would also like to thank one anonymous referee for his/her valuable comments that improved this paper.

References

[1] F. Cinti, P. Jain, M. Boninsegni, A. Micheli, P. Zoller and G. Pupillo, Supersolid droplet crystal in a dipole-blockaded gas, Phys. Rev. Lett., 105 (2010), 135301.

https://doi.org/10.4208/cicp.151214.021015a Published online by Cambridge University Press

[2] S. Saccani, S. Moroni and M. Boninsegni, Phase diagram of soft-core bosons in two dimensions, Phys. Rev. B, 83 (2011), 092506.
[3] N. Henkel, R. Nath and T. Pohl, Three-dimensional roton excitations and supersolid formation in Rydberg-excited Bose-Einstein condensates, Phys. Rev. Lett., 104 (2010), 195302.
[4] N. Henkel, F. Cinti, P. Jain, G. Pupillo and T. Pohl, Supersolid vortex crystals in Rydberg-dressed Bose-Einstein condensates, Phys. Rev. Lett., 108 (2012), 265301.
[5] C.-H. Hsueh, T.-C. Lin, T.-L. Horng and W. C. Wu, Quantum crystals in a Rydberg-dressed Bose-Einstein condensate, Phys. Rev. A, 86 (2012), 013619.
[6] P. Muruganandam and S. K. Adhikari, Bose-Einstein condensation dynamics in three dimension by the pseudospectral and finite-difference methods, J. Phys. B: At. Mol. Opt. Phys., 36 (2003), 2501–2513.
[7] K. Kasamatsu, M. Tsubota and M. Ueda, Vortex phase diagram in rotating two-component Bose-Einstein condensates, Phys. Rev. Lett., 91 (2003), 150406.
[8] K. Kasamatsu, M. Tsubota and M. Ueda, Structure of vortex lattice in rotating two-component Bose-Einstein condensates, Physica B, 329-333 (2003), 23–24.
[9] K. Kasamatsu, M. Tsubota and M. Ueda, Vortex states of two-component Bose-Einstein condensates with and without internal Josephson coupling, J. Low Temp. Phys., 134 (2004), 719–724.
[10] K. Kasamatsu and M. Tsubota, Vortex sheet in rotating two-component Bose-Einstein condensates, Phys. Rev. A, 79 (2009), 023606.
[11] J. J. García-Ripoll and V. M. Pérez-García, Optimizing Schrödinger functionals using Sobolev gradients: Applications to quantum mechanics and nonlinear optics, SIAM J. Sci. Comput., 23 (2001), 1316–1334.
[12] W. Bao and Q. Du, Computing the ground state solution of Bose-Einstein condensates by a normalized gradient flow, SIAM J. Sci. Comput., 25 (2004), 1674–1697.
[13] W. Bao, Ground states and dynamics of multi-component Bose-Einstein condensates, SIAM J. Multiscale Model. Simul., 2 (2004), 210–236.
[14] W. Bao, H. Wang and P. A. Markowich, Ground, symmetric and central vortex states in rotating Bose-Einstein condensates, Commun. Math. Sci., 3 (2005), 57–88.
[15] W. Bao, I.-L. Chern and F. Y. Lim, Efficient and spectrally accurate numerical methods for computing ground and first excited states in Bose-Einstein condensates, J. Comput. Phys., 219 (2006), 836–854.
[16] W. Bao and F. Y. Lim, Computing ground states of spin-1 Bose-Einstein condensates by the normalized gradient flow, SIAM J. Sci. Comput., 30 (2008), 1925–1948.
[17] I. Danaila and P. Kazemi, A new Sobolev gradient method for direct minimization of the Gross-Pitaevskii energy with rotation, SIAM J. Sci. Comput., 32 (2010), 2447–2467.
[18] W. J. F. Govaerts, Numerical Methods for Bifurcations of Dynamical Equilibria, SIAM Publications, Philadelphia, 2000.
[19] E. L. Allgower and K. Georg, Introduction to Numerical Continuation Methods, SIAM, Philadelphia, PA, 2003.
[20] H. B. Keller, Lectures on Numerical Methods in Bifurcation Problems, Springer-Verlag, Berlin, 1987.
[21] A. Jepson and A. Spence, Folds in solutions of two parameter systems and their calculation, Part I, SIAM J. Numer. Anal., 22 (1985), 347–368.
[22] W. C. Rheinboldt, Numerical Analysis of Parametrized Nonlinear Equations, Wiley, NY, 1986.
[23] W. C. Rheinboldt, On the computation of multidimensional solution manifolds of

https://doi.org/10.4208/cicp.151214.021015a Published online by Cambridge University Press

parametrized equations, Numer. Math., 53 (1988), 165–181.
[24] S.-L. Chang, C.-S. Chien and B.-W. Jeng, Tracing the solution surface with folds of a two-parameter system, Int. J. Bifurcation and Chaos, 15 (2005), 2689–2700.
[25] S.-L. Chang, C.-S. Chien and B.-W. Jeng, Computing wave functions of nonlinear Schrödinger equations: a time-independent approach, J. Comput. Phys., 226 (2007), 104–130.
[26] S.-L. Chang and C.-S. Chien, Adaptive continuation algorithms for computing energy levels of rotating Bose-Einstein condensates, Comput. Phys. Commun., 177 (2007), 707–719.
[27] G. L. Alfimov and D. A. Zezyulin, Nonlinear modes for the Gross-Pitaevskii equation–a demonstrative computation approach, Nonlinearity, 20 (2007), 2075–2092.
[28] D. A. Zezyulin, G. L. Alfimov, V. V. Konotop and V. M. Pérez-García, Control of nonlinear modes by scattering-length management in Bose-Einstein condensates, Phys. Rev. A, 76 (2007), 013621.
[29] D. A. Zezyulin, G. L. Alfimov, V. V. Konotop and V. M. Pérez-García, Stability of excited states of a Bose-Einstein condensates in an anharmonic trap, Phys. Rev. A, 78 (2008), 013606.
[30] H.-S. Chen, S.-L. Chang and C.-S. Chien, Spectral collocation methods using sine functions for a rotating Bose-Einstein condensation in optical lattices, J. Comput. Phys., 231 (2012), 1553–1569.
[31] S.-L. Chang and C.-S. Chien, Computing multiple peak solutions for Bose-Einstein condensates in optical lattices, Comput. Phys. Commun., 180 (2009), 926–947.
[32] Y.-S. Wang, B.-W. Jeng and C.-S. Chien, A two-parameter continuation method for rotating two-component Bose-Einstein condensates in optical lattices, Commun. Comput. Phys., 13 (2013), 442–460.
[33] C.-H. Hsueh, Y.-C. Tsai, K.-S. Wu, M.-S. Chang and W. C. Wu, Pseudospin orders in the supersolid phases in binary Rydberg-dressed Bose-Einstein condensates, Phys. Rev. A, 88 (2013), 043646.
[34] B.-W. Jeng, C.-S. Chien and I.-L. Chern, Spectral collocation and a two-level continuation scheme for dipolar Bose-Einstein condensates, J. Comput. Phys., 256 (2014), 713–727.

https://doi.org/10.4208/cicp.151214.021015a Published online by Cambridge University Press